scientific reports

Check for updates

OPEN

Green synthesis, characterization, and antimicrobial activity of silver nanoparticles from water-soluble fractions of Brazilian Kefir

Lucas Matos Martins Bernardes[1,4]✉, Serena Mares Malta[1,4], Ana Carolina Costa Santos[1], Rafael Alves da Silva[1], Tamiris Sabrina Rodrigues[1], Murillo Néia Thomaz da Silva[2], Vinicius Prado Bittar[3], Ana Luiza Silva Borges[3], Allisson Benatti Justino[3], Arlene Bispo dos Santos Nossol[2], Mário Machado Martins[2], Foued Salmen Espíndola[3], Ana Paula Mendes-Silva[4] & Carlos Ueira-Vieira[1]✉

Nanotechnology offers promising new avenues for combating drug-resistant pathogens. Given its antioxidant capacity, the water-soluble fraction of Brazilian kefir was hypothesized to serve as an effective reducing agent for the green synthesis of silver nanoparticles (AgNPs). It was further hypothesized that both the entire fraction (WSF) and the < 10 kDa fraction AgNPs would augment the therapeutic effects of kefir, particularly its antimicrobial activity. The successful synthesis was confirmed through the use of UV-Visible spectroscopy and Fourier-transform infrared analyses. WSF-AgNPs demonstrated potent antimicrobial activity, with minimum inhibitory concentrations of 25 µg/mL against *A. baumannii* ($p < 0.0001$) and 50 µg/mL against *K. pneumoniae* ($p < 0.0001$). Although no toxicity was observed in long-term tests on adult *Drosophila melanogaster*, AgNPs intake impaired larvae development. Oxidative stress analysis showed mild oxidative imbalance on advanced oxidation protein products (AOPP), sulfhydryl, and reduced glutathione (GSH) contents, with no alterations observed in reactive oxygen species (ROS) quantities, ferric reducing antioxidant power (FRAP), and catalase (CAT) activity. These findings suggest that kefir-derived AgNPs may have potential for combating drug-resistant infections. Future studies should focus on enhancing specificity through compound conjugation and investigating broader applications, including disinfectants, wound healing, and antibiotic development.

Keywords Silver nanoparticles, Kefir, Nanomedicine, Anti-bacterial agents

Abbreviations

2,4-DTBP	2,4-Di-tert-butylphenol
AgNPs	silver nanoparticles
AOPP	Advanced oxidation protein products
CAT	Catalase
DCFH-DA	Dichlorodihydrofluorescein diacetate
DLS	dynamic light scattering
DTNB	5,5'-Dithiobis(2-nitrobenzoic acid)
EDX	Energy-dispersive X-ray
FRAP	Ferric reducing antioxidant power
FT-IR	Fourier-transformed infra-red
GC-MS	Gas chromatography-mass spectrometry
GSH	Reduced glutathione
MIC	Minimum inhibitory concentration

[1]Genetics Laboratory, Institute of Biotechnology, Federal University of Uberlândia, Uberlândia, MG, Brazil. [2]Laboratory of Nanobiotechnology, Institute of Biotechnology, Federal University of Uberlândia, Uberlândia, Brazil. [3]Laboratory of Biochemistry and Molecular Biology, Institute of Biotechnology, Federal University of Uberlândia, Uberlândia, Brazil. [4]Department of Psychiatry, College of Medicine, University of Saskatchewan, Saskatoon, SK, Canada. ✉email: lucasmatosbernardes@hotmail.com; ueira@ufu.br

NPs	Nanoparticles
PA	Percent of activity
PBS	Phosphate-buffered saline
PDI	Polydispersity index
ROS	Reactive oxygen species
SEM	Scanning electronic microscopy
SOD	Superoxide dismutase
UV–Vis	Ultraviolet-visible spectroscopy
WSF	Kefir's whole water-soluble fraction

Nanotechnology is a rapidly advancing field that involves manipulating materials at the nanoscale, resulting in nanoparticles (NPs) ranging from 1 to 100 nm in size. These nanoparticles exhibit unique physicochemical properties and hold promise for addressing pressing health challenges[1]. In particular, the increase in the incidence of drug-resistant diseases poses a significant threat, with an estimated 700,000 deaths annually—a figure that is projected to increase to 10 million by 2050 if left unchecked[2]. Fungal infections are even more concerning, with more than 300 million people suffering from various fungal diseases, resulting in more than 2 million deaths annually from mycoses[2].

Silver nanoparticles (AgNPs) are particularly noteworthy in nanomedicine due to their exceptional antimicrobial efficacy and relatively low toxicity. AgNPs can potentially combat microbial resistance due to their unique properties, such as a high surface area-to-volume ratio and the ability to generate reactive oxygen species[2,3]. Therefore, exploring their antimicrobial activities could be a promising approach for addressing the growing threat of drug-resistant infections. One method for assessing the antimicrobial efficacy of AgNPs is through the disk diffusion technique, a reliable methodology that has been employed in numerous previous studies[4–7].

The NPs can be synthesized using physical, chemical, or biological methods. Although physical and chemical methods have traditionally been used for nanoparticle synthesis, their drawbacks, including cost, time consumption, and environmental concerns, have led to increased interest in biological synthesis methods[8–11].

Biological synthesis, also known as 'green synthesis,' uses nontoxic and eco-friendly reagents, offering a more streamlined approach to nanoparticle production. Organism-derived extracts, which are rich in biomolecules such as metabolites and proteins, play crucial roles as reducing and capping agents in this process[1,12]. This highlights the efficiency and versatility of biological synthesis. Studies have used cell-free extracts and derived substances from bacteria as precursors for nanoparticle synthesis[13,14].

In this context, kefir, a fermented beverage with well-documented antioxidant and antimicrobial properties, is a promising candidate for nanoparticle synthesis[15–18]. Although kefir has not been extensively studied in nanotechnology, our group has discovered significant antioxidant activity in the smaller than 10 kDa (< 10 kDa) fraction of the water-soluble component of kefir. Additionally, bioactive peptides have been identified from the this fraction[19,20]. Based on these findings, the water-soluble fraction (WSF) of kefir can be considered a promising agent for the green synthesis of nanoparticles.

Controlling the characteristics of the resulting nanoparticles in biological synthesis is challenging due to various factors that can impact the process, such as pH, temperature, and concentration of precursor agents[21]. Therefore, rigorous characterization of the NPs properties, including size, morphology, and chemical composition, is essential. Techniques such as UV-visible (UV–Vis) spectroscopy, Fourier transform infrared (FT-IR) spectroscopy, dynamic light scattering (DLS), and zeta potential measurements are well-described in the literature and provide valuable insights into these properties[10,22–24].

The potential toxicity of nanoparticles, particularly AgNPs, which are being developed for use in medical and antimicrobial applications, necessitates comprehensive evaluation through both in vitro and in vivo assays[25]. This is due to the possibility of increased interaction with human cells, which could lead to adverse effects. While the unique physicochemical properties of AgNPs may enhance antimicrobial efficacy, they may also raise concerns regarding cytotoxicity and long-term health effects. This highlights the necessity for rigorous toxicological assessments[26]. The fruit fly (*Drosophila melanogaster*) is a well-established model organism that offers several advantages, including a rapid life cycle, low cost of maintenance in laboratories, and a genome with significant human homology[27]. This model has been previously utilized for studies on the toxicity of AgNPs, examining aspects such as lifespan and gut morphology[28–30]. Consequently, the model is a reliable means of assessing the safety of AgNPs, facilitating the generation of preliminary insights that can inform subsequent preclinical testing.

This study aimed to examine the potential of kefir for nanoparticle synthesis and its antimicrobial applications. First, we analyzed the water-soluble fraction of kefir as a reagent for nanoparticle synthesis. We then characterize the synthesized nanoparticles including size, morphology, and chemical composition. Additionally, we assessed their antimicrobial activity by determining their minimum inhibitory concentration against a set of multidrug-resistant bacteria. Moreover, we evaluated the toxicity of AgNPs by using fruit flies. This research aimed to contribute to the advancement of the use of nanotechnology in healthcare, more specifically the potential of kefir-derived silver nanoparticles in antimicrobial activities.

Materials and methods

Kefir production and collection of its water-soluble fractions

The kefir grains utilized in this study were donated by residents of the city of Uberlândia, Brazil. The grains were previously characterized through genetic fingerprinting by our group[20]. To produce kefir, whole cow's milk was fermented with a 10% (w/v) concentration of kefir grains. Fermentation occurred over a 24-hour period at a

controlled temperature of 28 °C, shielded from light. Following fermentation, the kefir was separated from the grains using a sieve.

To obtain the water-soluble fraction (WSF), the kefir was centrifuged twice at 4900*g* for 10 min at 4 °C. After each centrifugation, the supernatant was collected, and the pellet was discarded. Then, the resulting supernatant was filtered through two layers of filter paper[20].

To ensure the suitability of the WSF for nanoparticle synthesis, we modified the protocol[20]. Specifically, we added ammonium hydroxide (NH_4OH) to the WSF immediately after filtration at a concentration of 0.05% v/v. This addition aimed to alter the pH of the sample and precipitate proteins that might interfere with nanoparticle synthesis. Subsequently, we centrifuged the solution at 12000*g* for 15 min at 4 °C to pellet the proteins, which enabled us to collect the clarified supernatant for nanoparticle synthesis. The NH_4OH is usually added during the nanoparticle synthesis process, but the protocol required adaptation due to an unsuccessful first synthesis (explained in the Results section).

Furthermore, the supernatant underwent further filtration using a vacuum pump and a 0.22 µm membrane. Subsequently, it was purified through a 10 kDa Amicon column to fractionate the WSF into the smaller than 10 kDa (< 10 kDa) fraction.

Green synthesis of silver nanoparticles from Kefir fractions

The silver nanoparticles synthesis method employed in this study was modified from a previous described green synthesis protocol[31]. First, we added 60 mL of each fraction (whole WSF and < 10 kDa), which already contained NH_4OH, to individual flasks containing 0.18 g of silver nitrate ($AgNO_3$). The flasks were briefly shaken and then heated to boiling in a microwave oven. Upon reaching the boiling point, the solutions turned brown, indicating the formation of nanoparticles. Each solution was stirred using a magnetic stirrer for 15 min at medium speed.

After the synthesis process, the nanoparticles were subjected to three cycles of centrifugation (16000*g*, 15 min, 4 °C). After each cycle, the supernatant was discarded, and the pellet containing the silver nanoparticles was resuspended in deionized water. The resulting solution was stored in a refrigerator set at 4 °C. To determine the concentration of each solution, a portion was air-dried and weighed. The nanoparticles derived from the WSF and < 10 kDa fractions are referred to as WSF-AgNPs and < 10 kDa-AgNPs, respectively.

Gas Chromatography-Mass spectrometry (GC-MS) for WSF characterization

A GC-MS analysis was performed on a protein-free sample of the WSF. For sample preparation, 100 µL of WSF were mixed with 1 mL of a solution composed of acetonitrile, isopropanol, and water in a 3:3:2 ratio. The mixture was centrifuged at 10,000 rpm for 10 min, resulting in the formation of a protein pellet. The supernatant was collected and dried overnight under reduced pressure. The resulting dried residue was resuspended in 100 µL of HPLC-grade dichloromethane.

A 6 µL aliquot of the prepared solution was injected into an Agilent 7890B GC system operated in split mode (1:1). Metabolite separation was achieved using an HP5-MS UI capillary column (Agilent #19091S-433UI) with helium as the carrier gas at a flow rate of 0.82 mL/min. The injector temperature was maintained at 250 °C. The column temperature program was initiated at 60 °C, held for 1 min, then increased at 10 °C/min to 310 °C over 37 min. The column effluent was introduced into the ion source of an Agilent 5977 A mass selective detector operating in electron impact ionization mode (70 eV).

Mass spectra acquisition commenced after a solvent delay of 6.5 min. Spectra were recorded at a scan rate of 2.9 scans per second over an m/z range of 50–550 with a step size of 0.1 m/z. The temperatures of the MS quadrupole and ion source were set to 180 °C and 280 °C, respectively. Data analysis was performed using Total Ion Chromatography (TIC) with a minimum match factor threshold of 75%. Compound identification was based on comparisons of mass spectra and retention times with the NIST library (2017) using Agilent MassHunter Unknowns Analysis 10.0 software (https://www.agilent.com).

Characterization of silver nanoparticles

Analytical techniques, including UV–Vis, DLS, for size measurements and zeta potential analysis, and FT-IR were used to characterize the silver nanoparticles. UV–Vis spectroscopy was employed to analyze characteristics of the nanoparticles, and the efficiency of their synthesis based on the absorbance peak (typically 400–500 nm) of silver nanoparticles. In a 96-well plate, triplicate samples (100 µL each) of nanoparticle solutions, along with WSF and silver nitrate controls, were analyzed. Spectra were measured from 300 to 800 nm using a standardized UV–Vis spectrophotometer. Analysis of the data included peak identification based on wavelength and intensity criteria. Triplicate samples were used to ensure the reliability of the results.

The infrared spectra of the AgNPs and their precursors were obtained using an Agilent Cary 630 FTIR spectrophotometer in the range from 4000 to 650 cm^{-1}. Sample analyses were performed in the solid state using the Attenuated Total Reflectance (ATR) accessory with a diamond crystal.

The initial step of the DLS analysis involved optimizing the measurements for each sample. Nanoparticle solutions were prepared at a range of concentrations from 0.01 mg/mL to 5 mg/mL. Subsequently, size distribution, hydrodynamic radius, and polydispersity index of the nanoparticles were evaluated in quintuplicate. Each measurement was conducted at 25 °C using 2 mL of sample. To ensure stable measurements, a 3-minute equilibrium time was implemented, allowing the nanoparticles to reach a steady state and match the equipment's temperature. The backscatter measurement angle (175°) was chosen due to its high sensitivity to minute particles and its ability to minimize the impact of multiple scattering, thus ensuring reliable and precise data on size distribution.

The optimization process aimed to determine the nanoparticle concentration that would consistently yield reliable results in five replicates. We considered parameters provided by the DLS equipment (Litesizer 500, Anton Paar, UK), such as baseline, $g1^2$, and transmittance values, to ensure accurate measurements. Adhering

to recommended criteria is crucial for obtaining reliable data. Our analysis focused on two parameters: transmittance levels and baseline values. Based on manufacturer guidelines, transmittance levels should ideally exceed 80%, with values above 60% considered acceptable. Baseline values should remain at 1 for optimal performance.

The DLS equipment was also used for examining the zeta potential of the AgNPs, which was measured in quintuplicate at 0.1 mg/mL for WSF-AgNPs and 0.05 mg/mL for the < 10 kDa-AgNPs. The measurements were made using 200 V at 25 °C with an equilibrium time of 3 min. The reasoning for selecting these concentrations for the analysis will be further discussed in the Results section.

A scanning electron microscopy (SEM) analysis was conducted to corroborate the data obtained from the DLS analysis regarding the dimensions of the nanoparticles and to gather additional information on their morphology. A Vega 3 TESCAN scanning electron microscope, operated at 20 kV and equipped with a secondary electron detector and an energy-dispersive X-ray (EDX) detector (Oxford Instruments, Bucks, England), was utilized for this analysis. Prior to imaging, the synthesized AgNPs were dispersed in an ultrasonic bath for five minutes to ensure a homogeneous suspension and prevent agglomeration. A small aliquot of the suspension was then drop-cast onto a clean silicon wafer substrate, providing a conductive surface that minimizes charging effects during SEM operation. The samples were then left to air-dry at room temperature to evaporate the solvent, thereby ensuring proper adhesion of the nanoparticles to the substrate for optimal imaging conditions.

In vitro susceptibility test (disk diffusion method)

The anti-bacterial property of AgNPs was evaluated using a diffusion disk test against eight strains of multidrug-resistant bacteria, including *Acinetobacter baumannii*, *Escherichia coli* (MCR), *Klebsiella pneumoniae carbapenemase*, three strains of *Pseudomonas aeruginosa* (IMP, VIM, and SPM), and *Staphylococcus aureus* (MRSA), obtained from the Molecular Microbiology Laboratory of the Federal University of Uberlândia. Strain characterization was performed by bacterial genotyping by PCR and phenotyping on ampicillin and polymyxin supplemented BHI agar. The modified Kirby-Bauer disk diffusion method was used to assess antimicrobial activity[32,33].

For testing, bacteria were plated on agar plates at a concentration of 0.5 on the McFarland scale. Subsequently, 15 µL of AgNPs at three concentrations (10, 100 and 1000 µg/mL) were applied to antimicrobial susceptibility test discs in triplicate. The discs were incubated at 37 °C for 24 h and then examined for the presence of inhibition zones, with halo diameters measured using calipers.

Minimum inhibitory concentration (MIC)

The MIC assay was performed on bacteria that showed inhibition by AgNPs at 100 µg/mL in preliminary in vitro susceptibility testing, following a protocol by Bio-Rad Antibodies[34]. For WSF-AgNPs, the assay included *A. baumannii* and *K. pneumoniae*, while for < 10 kDa-AgNPs, it included *A. baumannii*, *K. pneumoniae*, *E. coli*, and *S. aureus*. Serial dilutions of AgNPs were prepared in the range of 100 µg/mL to 3.12 µg/mL using 96-well plates. Each well was filled with 100 µL of bacterial suspension and 100 µL of AgNP dilutions in sextuplicate.

Positive controls consisted of bacterial suspensions in LB medium without AgNPs, while negative controls contained only LB medium to ensure sterility. Plates were incubated for 24 h at 37 °C. After incubation, 20 µL of 0.6 mM resazurin dye was added to each well. Resazurin acts as a viability indicator and changes color in the presence of metabolically active bacteria. Plates were again incubated for 1 to 3 h or until a color change was observed. Antimicrobial activity was determined by measuring the absorbance at 570 nm and 600 nm using a microplate reader.

Toxicity assessment

The evaluation of toxicity was conducted in two phases. The initial step involved the assessment of post-embryonic developmental toxicity in *Drosophila melanogaster*. Flies of the mutant strain w^{1118} (BL #3605) were placed on an oviposition substrate prepared with fresh biological yeast and refined sugar for a period of 12 h to facilitate egg laying. The embryos were subsequently collected using a fine brush and sieve. Approximately 100 embryos were transferred into individual vials containing 0.5 g of instant culture medium. This medium was prepared with 2.3 mL of distilled water and consisted of 75% instant potato puree, 15% yeast extract, 9.3% glucose, and 0.07% nipagin. Each vial's medium surface was treated with 200 µL of one of the experimental conditions, which included distilled water, WSF, and $AgNO_3$ at concentrations of 1, 10, and 100 µg/mL. The concentrations of WSF-AgNPs and < 10 kDa-AgNPs were 1, 10, and 100 µg/mL, respectively. Each treatment was conducted using a single vial. The vials were maintained in a BOD incubator at a controlled temperature of 25 °C under a 12:12 light-dark cycle. The emergence of adults was observed over a seven-day period following the first emergence, and the number of individuals was recorded.

Subsequently, the toxicity of the treatments was assessed using adult flies of the same strain aged between 0 and 2 days post-emergence. Twenty adult flies (ten males and ten females) were placed in vials containing the same treatments as in the developmental study. Each treatment was conducted in triplicates. The methodology for the application of the treatments remained consistent throughout the experiment, with 200 µL of each condition applied to the surface of the instant culture medium. The medium was replaced every two days to ensure a continuous supply of fresh food and treatment. At each replacement, the number of dead flies was recorded. The total exposure duration was 15 days.

Oxidative stress analysis

In the same manner as the post-embryonic development toxicity assessment, *Drosophila melanogaster* embryos, of the mutant strain w^{1118} (BL #3605), were collected and placed in vials containing the aforementioned

treatments. After five days, triplicates of 40 L3-stage larvae were collected from each treatment vial, transferred to microtubes, and preserved at −80 °C until biochemical analyses were conducted.

The oxidative stress biochemical analysis was conducted to quantify the following parameters: reactive oxygen species (ROS), ferric reducing antioxidant power (FRAP), advanced oxidation protein products (AOPP), sulfhydryl group content, superoxide dismutase (SOD) activity, catalase (CAT) activity, and reduced glutathione (GSH) content. Each group of larvae was homogenized in phosphate buffer (1:10 w/v, pH 7.4). Subsequently, the homogenates were centrifuged at 800 g for 10 min at 4 °C, and the supernatants were collected for analysis. Total protein content in the samples was determined using the Bradford method, using an analytical curve made with bovine serum albumin as standard[35]. All assays were performed in biological triplicates and technical duplicates. Absorbance and fluorescence measurements were conducted using a Perkin-Elmer LS 55 Fluorescence Spectrometer.

ROS quantification

The quantification of ROS was conducted in accordance with the methodology described by Myers et al., 2018[36]. In brief, the homogenates were incubated with dichlorodihydrofluorescein diacetate (DCFH-DA) at a concentration of 10 µM and Tris-HCl buffer (5 mM, pH 7.4) for three minutes. The absorbance of the samples was then measured in 96-well plates at a wavelength of 530 nm, with excitation at 474 nm.

FRAP method

The FRAP assay was conducted by sampling 10 µL from the homogenates, incubating the samples with acetate buffer (0.3 M, pH 3.6), 2,4,6-tri(2-pyridyl)-s-triazine acidic solution at 10 mM, and ferric chloride at 20 mM at 37 °C for six minutes. Subsequently, the absorbance was quantified at 593 nm, with the antioxidant capacity ascertained through the construction of a standard curve employing Trolox at concentrations spanning from 0 to 1000 µM. The results were expressed as µmol trolox eq/mg of protein.

AOPP quantification

The determination of AOPP was conducted in accordance with the methodology delineated by Witko-Sarsat et al., 1996[37]. A spectrophotometer was utilized, with calibration conducted using a chloramine-T solution that exhibits absorption at 340 nm in the presence of potassium iodide. For the purpose of sample analysis, 20 µL of homogenate were combined with 160 µl of phosphate-buffered saline (PBS) and 20 µl of citric acid. The standard curve was prepared using chloramine-T and potassium iodide (1.16 M). To each 200 µL standard solution, 10 µL of potassium iodide and 20 µL of citric acid were added, followed by shaking the plate for six minutes. Absorbance at 340 nm was then measured.

Sulfhydryl group content quantification

The quantification of sulfhydryl groups (free thiols) was conducted based on a method by Ellman, 1959[38], utilizing 5,5'-dithiobis(2-nitrobenzoic acid) (DTNB) as the analytical reagent. Homogenates (50 µL) were combined with 30 µL of a 10 mM DTNB solution prepared in potassium phosphate buffer (pH 8.0) and incubated for 30 min. The absorbance was recorded at 412 nm, and the free thiol concentration was calculated using a molar extinction coefficient of 14,150 $M^{-1}.cm^{-1}$.

SOD activity quantification

The assessment of SOD activity was conducted in the manner described by Marklund and Marklund, 1974[39]. Samples from the homogenates, 15 µL, were collected and combined with 80 U/mL catalase and 24 mM pyrogallol, diluted in 50 mM Tris-HCl buffer containing 1 mM EDTA at pH 8.2. The kinetic analysis was performed on a 96-well plate over a 10-minute period at a wavelength of 420 nm. To quantify SOD enzymatic activity, a calibration curve was prepared using SOD as a reference standard.

CAT activity quantification

The assessment of CAT activity was conducted in reference to the methodology proposed by Aebi, 1984[40], with minor modifications. Samples containing 50 µL of the homogenates were incubated with 10% Triton X-100, followed by the addition of a 0.2% hydrogen peroxide (H_2O_2) solution diluted in 10 mM phosphate buffer. The kinetic analysis was performed on a 96-well plate over a 10-minute period at a wavelength of 240 nm.

GSH content

The quantification of GSH proceeded with the homogenates being treated with metaphosphoric acid (1:1) in order to precipitate the proteins. The resulting mixture was then subjected to centrifugation at 7,000 rpm for 10 min, after which the supernatant was collected. Subsequently, sodium phosphate buffer and o-phthalaldehyde (1 mg/mL, dissolved in methanol) were added to the supernatant. The fluorescence intensity was then measured in a 96-well plate with excitation and emission wavelengths of 350 nm and 420 nm, respectively. A standard curve was constructed using GSH as a reference, thereby enabling the determination of the GSH content in the samples.

Statistical analysis

The statistical analysis was performed using the GraphPad Prism 9.0 software (https://www.graphpad.com). To evaluate data normalization, we used the Shapiro–Wilk test. For DLS optimization, we carried out a one-way ANOVA with Tukey's multiple comparison or the Kruskal–Wallis for continuous variables with normal or non-normal distribution, respectively. The statistical analysis for the disk diffusion assay was conducted using a two-way ANOVA with Tukey's multiple comparison test. The toxicity assay was analyzed using the Mantel-Cox

statistical test. The MIC and oxidative stress analyses were performed using a one-way ANOVA followed by Dunnett's multiple comparisons post-test. A significance of $p \leq 0.05$ was applied for statistical threshold.

Results

Green synthesis of silver nanoparticles from Kefir fractions

In our first attempt at synthesis, the protocol required the addition of NH_4OH after mixing the WSF with $AgNO_3$. However, this sudden change in pH, from 4.2 (prior to the NH_4OH addition) to 9.98, caused the precipitation of large proteins from the WSF. As a result, during the subsequent washing process, these proteins formed a separate pellet on top of the AgNPs pellet, making it difficult to effectively wash and recover the AgNPs.

To address the issue, we introduced NH_4OH during the fractionation of the WSF, just before filtration through a 0.45 µM filter. This addition facilitated the precipitation of large proteins, which were then easily removed by centrifugation. By collecting the supernatant, the synthesis process could proceed smoothly avoiding challenges associated with washing.

GC-MS analysis

The GC-MS analysis of WSF (Fig. 1) revealed a diverse range of compounds spanning various chemical families, including fatty acids, long-chain fatty alcohols, aromatic compounds, phenols, and steroids. Notably, five distinct fatty acids and ten long-chain fatty alcohols were identified. The two most abundant compounds were n-hexadecanoic acid (palmitic acid) with a retention time of 17.722 min and octadecanoic acid (stearic acid) with a retention time of 19.610 min. Both compounds are naturally present in milk and, consequently, in kefir.

Additionally, fermentation-specific compounds, such as fatty amides and phenols, were identified. Among these, kefir-specific compounds of particular interest include 2,4-di-tert-butylphenol, 1-heptadecanamine, and 9-octadecenamide (Z)-, which were present in higher abundance in the samples. Their respective retention times were 12.852, 19.805, and 21.384 min. A comprehensive list of the WSF components is provided in the Supplementary Material 1.

Characterization of silver nanoparticles

Following the green synthesis of kefir AgNPs, we performed the analysis of nanoparticle absorbance within the ultraviolet-visible spectra revealed a distinct absorbance peak between 400 and 500 nm, specifically at 470 nm,

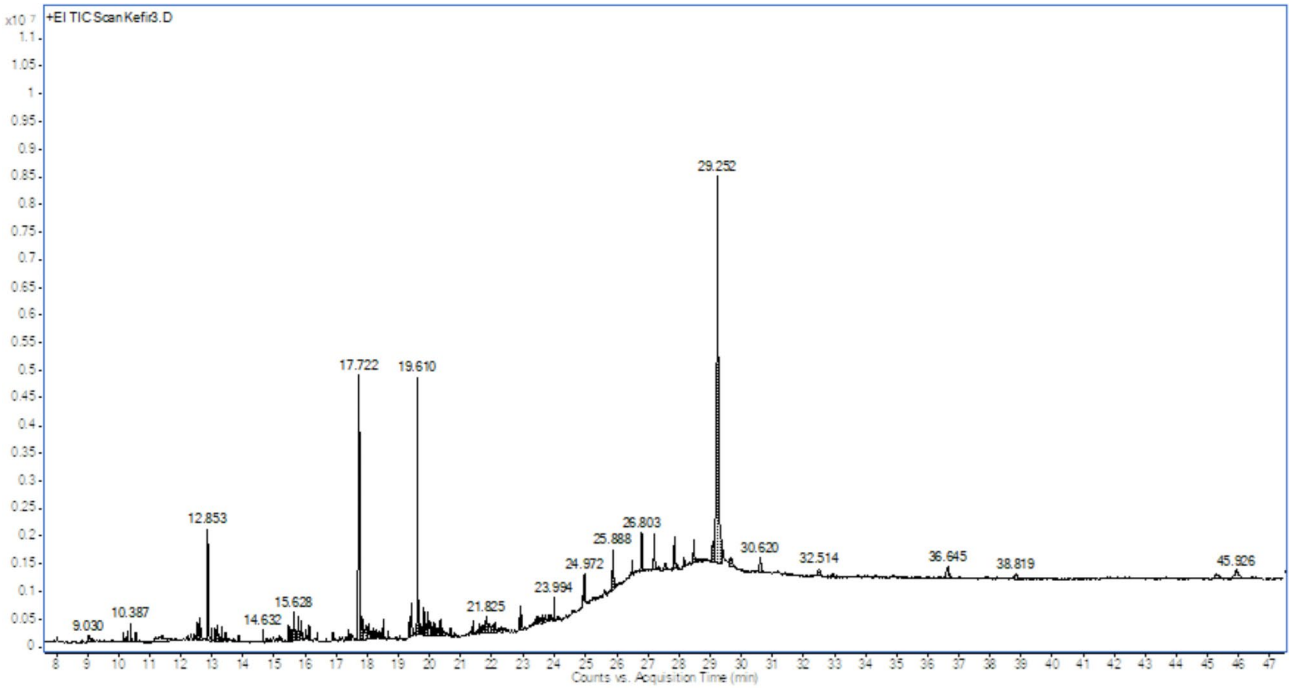

Fig. 1. GC-MS chromatogram of WSF. A diverse range of compounds was identified in WSF using GC-MS analysis. The majority of the identified compounds belong to the fatty acid chemical family, including *n*-hexadecanoic acid (retention time: 17.722 min) and octadecanoic acid (retention time: 19.610 min). Additionally, long-chain fatty alcohols, aromatic compounds, phenols, and steroids were detected. Both *n*-hexadecanoic acid and octadecanoic acid are known to be present in milk and, consequently, in kefir. Furthermore, several compounds directly associated with fermentation processes were identified, among which the three most abundant are 2,4-di-tert-butylphenol (retention time: 12.825 min), 1-heptadecanamine (retention time: 19.805 min), and 9-octadecenamide (Z)- (retention: 21.384 min). These results underscore the intricate biochemical composition of kefir.

exclusively in the WSF-AgNPs. No distinct absorbance peaks were observed in the $AgNO_3$ solution, the WSF, or the nanoparticles from the < 10 kDa fraction (Fig. 2).

The results of the FT-IR analysis (Fig. 3) showed significant peaks in various regions. In the 3000–3500 cm^{-1} range (labeled A), WSF exhibited a peak that corresponds to N-H and O-H functionalities. Additionally, within the 1500–1700 cm^{-1} range (labeled B), distinct peaks indicated the presence of C = O stretching vibration and trivalent nitrogen, observed in both WSF and AgNPs spectra. The WSF exhibited two peaks in the 1000–1300 cm^{-1} range (labeled C), indicative of the presence of C-O and C-N bonds. The analysis validates the successful synthesis of AgNPs using WSF as a precursor, as indicated by the matching peaks found in both WSF and the AgNPs.

On the DLS optimization, the transmittance of the WSF-AgNPs samples started to decrease at a concentration of 0.5 mg/mL, falling below the recommended threshold, and reached 0% at a concentration of 5 mg/mL (Fig. 4A). Among the first three concentrations—those that had satisfactory transmittance values—the 0.1 mg/mL concentration was closest to achieving a baseline value of 1 (Fig. 4B).

During the analysis of < 10 kDa-AgNPs, the transmittance started to decrease at a concentration of 0.05 mg/mL and reached 0% at a concentration of 1 mg/mL (Fig. 4C), while the baseline stabilized at a concentration of 0.1 mg/mL, yielding a value closer to the recommended value (Fig. 4D).

Given that the DLS technique is dependent on light passing through the sample and reaching the detector, maintaining transmittance values above the recommended threshold was of primary importance. Therefore, for subsequent analyses of hydrodynamic radius, polydispersity index (PDI), and zeta potential, a concentration of 0.1 mg/mL was selected for WSF-AgNPs, and 0.05 mg/mL was chosen for the < 10 kDa-AgNPs, based on optimization data from DLS analysis.

The DLS measurements reported that the WSF-AgNPs exhibited only one peak between 500 and 1000 nm, indicating the presence of only nanoparticles within this size range in the sample. The < 10 kDa-AgNPs showed a predominance of nanoparticles smaller than 100 nm in their samples but also a small quantity of larger nanoparticles (Fig. 5A).

The hydrodynamic radius of the WSF-AgNPs was approximately 1201 nm, while for the < 10 kDa-AgNPs it was approximately 481 nm (Fig. 5B). For the WSF-AgNPs, the PDI was approximately 50%, while for the < 10 kDa-AgNPs, it was 28,63% (Fig. 5C). Finally, the mean zeta potential for all nanoparticle samples was approximately – 30 mV (Fig. 5D).

The SEM analysis validated the findings observed in the DLS. The WSF-AgNPs have a spherical-like shape and exhibited a size range of 500 to 1000 nm (Fig. 6A), whereas the < 10 kDa-AgNPs demonstrated a smaller size range of 100 to 200 nm, with some nanoparticles measuring approximately 400 nm, with a spherical-like shape, with the exception of the larger AgNPs, that have a cubic shape (Fig. 6C). The EDX results revealed the presence of carbon, silicon, chloride, and silver atoms on both AgNPs (Fig. 6B and D). Given that silver is the primary material utilized in nanoparticle synthesis and silica was the substrate employed for the analysis, it can be inferred that the carbon and chloride originate from the molecules present in the water-soluble fraction of kefir.

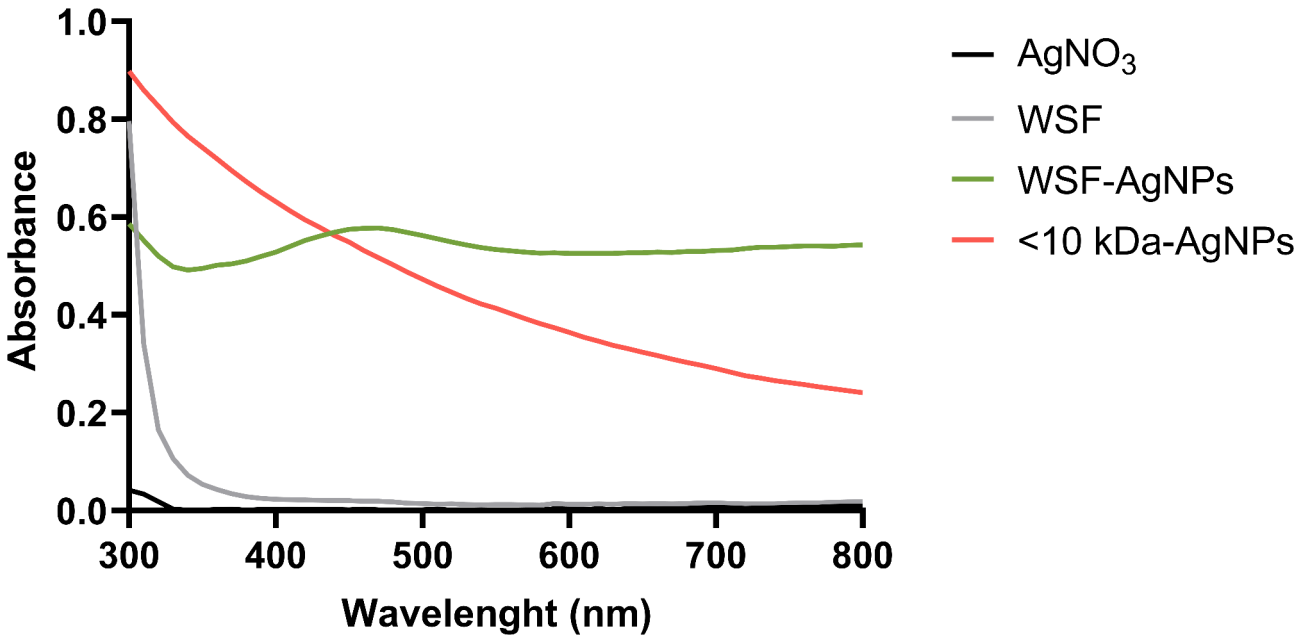

Fig. 2. UV–visible spectroscopy. $AgNO_3$ and WSF did not exhibit any absorbance within this spectral range. The WSF-AgNPs exhibited an absorbance peak at 470 nm, as anticipated for AgNPs. The < 10 kDa-AgNPs did not show an absorbance peak within this spectrum, but their absorbance was not insignificant. The samples were evaluated in triplicate.

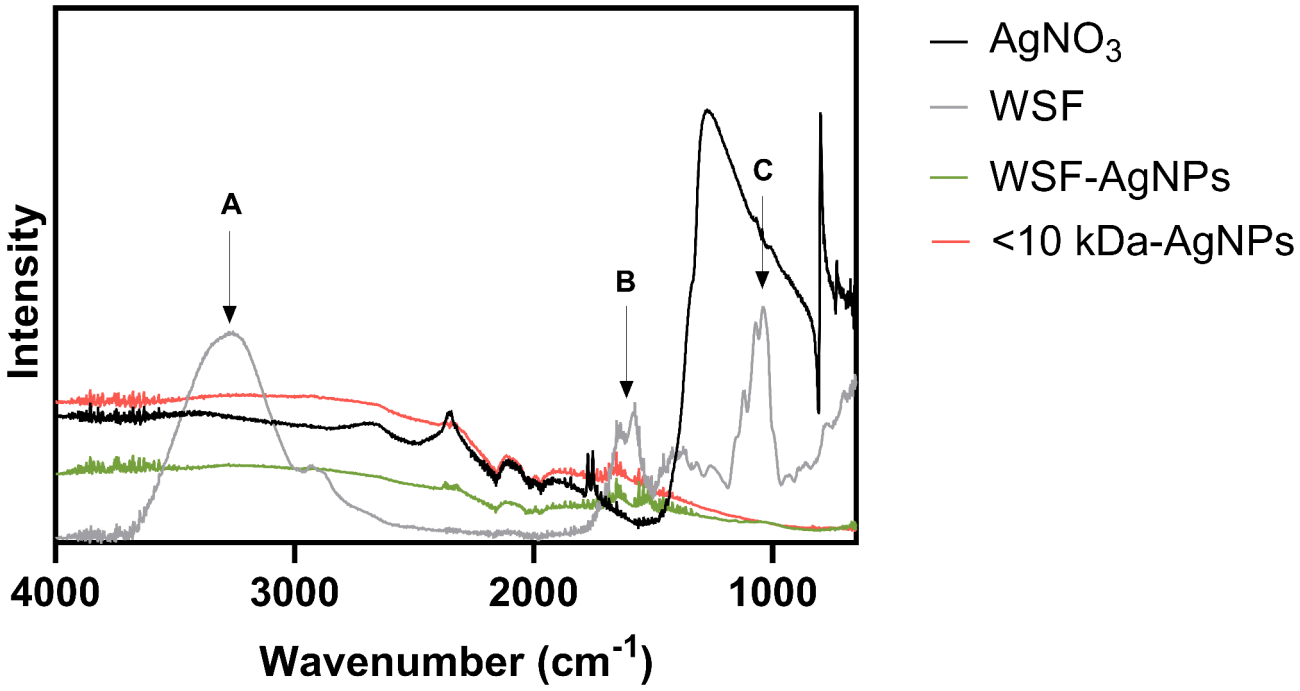

Fig. 3. **FT-IR spectroscopy.** During the FT-IR analysis, matching peaks were observed between the AgNPs and their precursors, $AgNO_3$ and WSF. Transmittance peaks were reported for WSF at the N-H and O-H functionalities region (A), C = O and trivalent nitrogen region (B) and C-O and C-N bonds region (C). Matching peaks were observed for the WSF and AgNPs on the region labeled B. These results suggest that the silver nanoparticles synthesis was successful, due to the precursor and the AgNPs sharing similar chemical bonds in their composition.

In vitro susceptibility test (disk diffusion method)

The investigation of in vitro susceptibility of bacteria through disk diffusion (Table 1) showed that only *A. baumannii* was inhibited by the WSF alone. The WSF-AgNPs at 10 µg/mL did not inhibit the growth of any of the tested multidrug-resistant bacteria. Increasing the concentration to 100 µg/mL resulted in inhibitory effects observed on *K. pneumoniae* and *A. baumannii* ($p < 0.0001$). At a concentration of 1000 µg/mL, the WSF-AgNPs exhibited inhibitory activity against all the tested bacterial strains.

At a concentration of 10 µg/mL, there was no inhibition zone for the < 10 kDa-AgNPs. However, at 100 µg/mL, inhibition zones were observed against *A. baumannii*, *E. coli*, *K. pneumoniae*, and *S. aureus* ($p < 0.0001$). Notably, complete growth inhibition was evident at a concentration of 1000 µg/mL against all multidrug-resistant bacteria evaluated. Pictures of the plates where the disk diffusion assays were conducted can be found in Supplementary Material 2, alongside a graphical representation of the obtained results.

Minimum inhibitory concentration

In the MIC assays, WSF-AgNPs demonstrated efficacy in inhibiting the growth of *A. baumannii* at concentrations of 100, 50, and 25 µg/mL ($p > 0.0001$) (Fig. 7A), while exhibiting a similar inhibitory effect on *K. pneumoniae* at 100 and 50 µg/mL ($p > 0.0001$) (Fig. 7B). Consequently, the minimum inhibitory concentrations were identified as 25 µg/mL for *A. baumannii* and 50 µg/mL for *K. pneumoniae*. Colorimetric analysis using resazurin demonstrated that at these concentrations, the nanoparticles exhibited bactericidal effects against both tested bacteria.

In contrast, 10 kDa-AgNPs, despite exhibiting inhibition zones in the disk diffusion assay at 100 µg/mL, did not replicate this effect in the MIC assay, either at the initial concentration of 100 µg/mL or at subsequent dilutions. The experiment was repeated twice using different batches of nanoparticles from separate syntheses, but the results were inconsistent across both repetitions, suggesting potential instability under MIC assay conditions.

Toxicity assessment

The toxicity assessment during post-embryonic development on *Drosophila melanogaster* demonstrate a concentration-dependent toxicity of $AgNO_3$ and AgNPs (Table 2). At a concentration of 100 µg/mL, $AgNO_3$ was found to completely inhibit adult emergence, with a p-value of less than 0.0001, thereby demonstrating severe toxicity. Similarly, both WSF-AgNPs and < 10 kDa-AgNPs at 100 µg/mL significantly reduced the number of emerging adults ($p = 0.0146$ and $p = 0.0031$, respectively), indicating a high level of toxicity. At a concentration of 10 µg/mL, $AgNO_3$ demonstrated moderate toxicity, with a significantly reduced number of adults emerging compared to the water control ($p = 0.0448$). It is noteworthy that WSF-AgNPs at 10 µg/mL demonstrated a

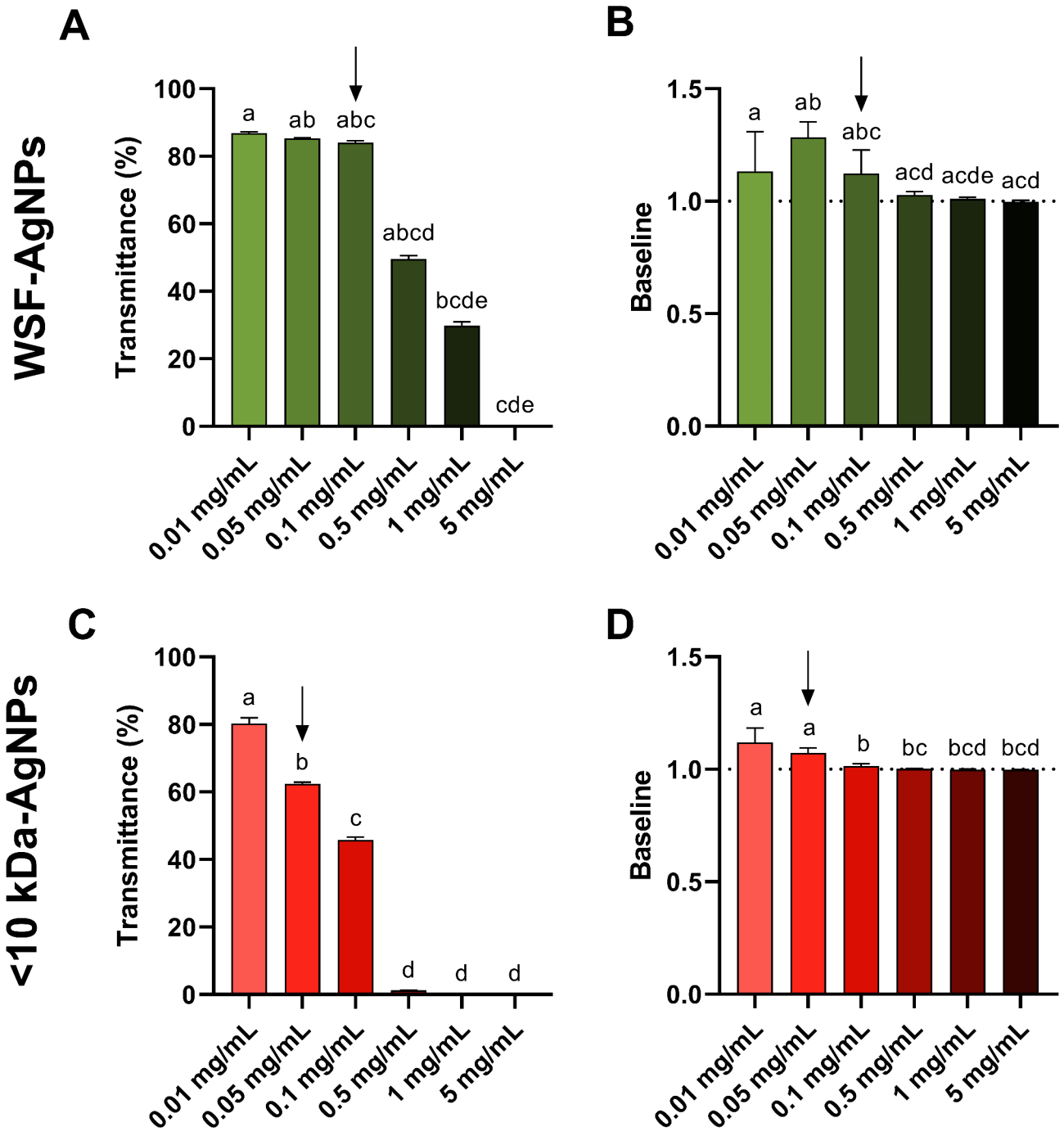

Fig. 4. **DLS Optimization.** When conducting DLS, it is important to ensure that the transmittance values are not below 60% and the baseline is close to 1. For WSF-AgNPs, only concentrations of 0.01, 0.05, and 0.1 mg/mL (A) had acceptable transmittance values. However, the baseline was closer to the reference value at the 0.1 mg/mL concentration (B). For the < 10 kDa-AgNPs, only the concentrations of 0.01 and 0.05 mg/mL provided transmittance values above the reference value (C). However, the baseline values for the 0.05 mg/mL concentration group were closer to the ideal value (D). The data normalization was evaluated using the Shapiro–Wilk test. Statistical differences were evaluated using one-way ANOVA after normalizing the data. If the data did not pass the normality test, Kruskal–Wallis test was used to calculate significant differences. In both cases, multiple comparisons were made using Tukey's test. The concentrations that displayed the most appropriate values for each parameter are indicated by the arrows. Data is presented as mean ± standard deviation.

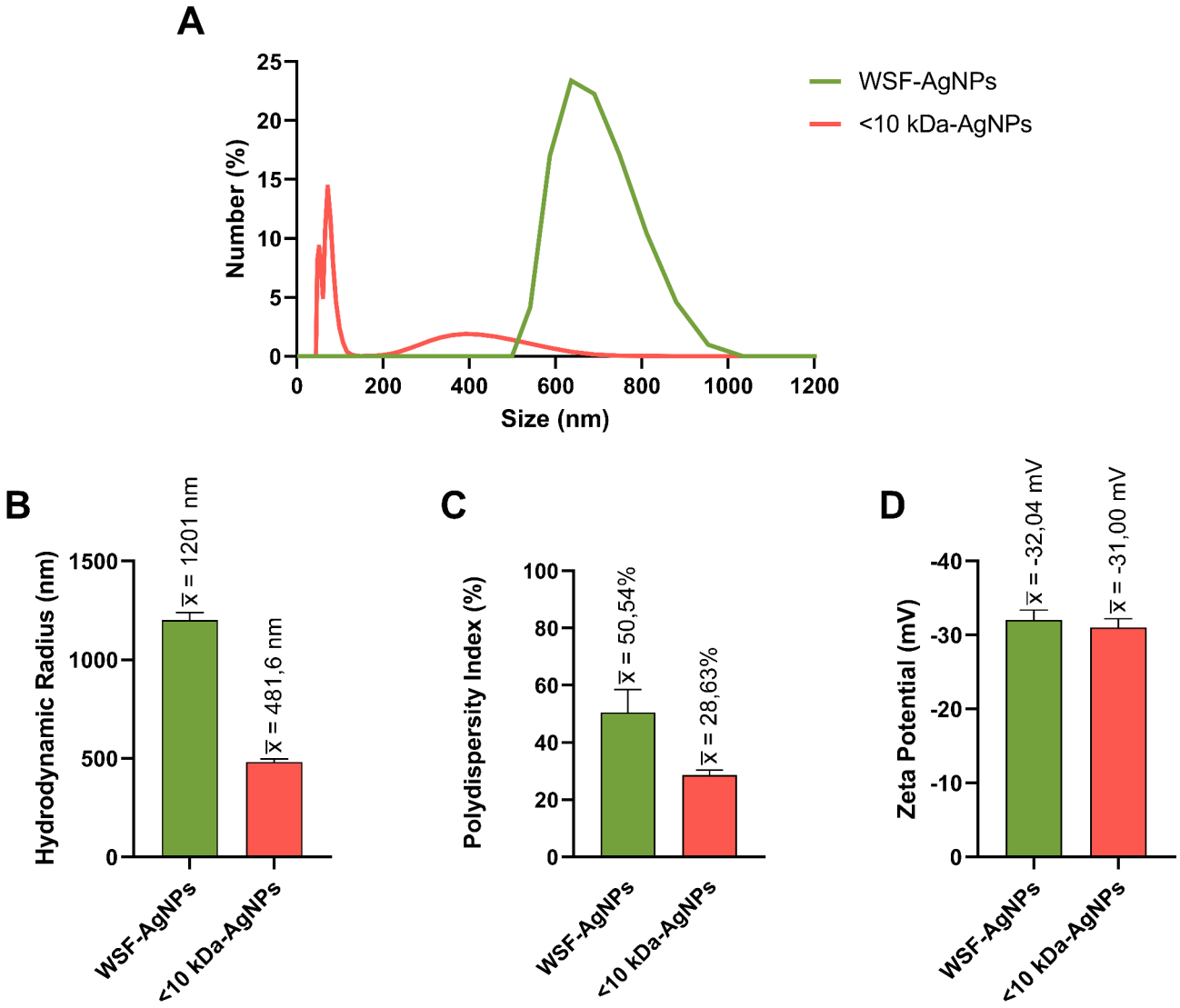

Fig. 5. **DLS size measurements and zeta potential.** The size measurement analysis for the WSF-AgNPs reported particles between 500 and 1000 nm being the only ones present in the sample. For the < 10 kDa-AgNPs, the majority had sizes less than 100 nm (**A**). The hydrodynamic radius of the WSF-AgNPs was approximately 1201 nm, while for the < 10 kDa-AgNPs it was 481,6 nm (**B**). The WSF-AgNPs had a polydispersity index of 50%, while the < 10 kDa-AgNPs had a PDI of 30% (**C**). The mean zeta potential for all nanoparticles was lower than − 30 mV (**D**). Data on graphs B, C, and D are presented as mean ± standard deviation.

tendency towards enhanced adult emergence in comparison to the control ($p = 0.0979$), indicating a potential protective effect, although this was not statistically significant. At the lowest concentration (1 µg/mL), no significant differences in adult emergence were observed between the treatments, including $AgNO_3$, WSF-AgNPs, and < 10 kDa-AgNPs, and the water control ($p > 0.05$). These findings suggest that both silver nanoparticles and silver nitrate exhibit toxic effects at higher concentrations, with nanoparticles demonstrating relatively less pronounced toxicity at intermediate levels.

In the case of adult flies, no treatment demonstrated a higher mortality rate in comparison to the control group, with the exception of AgNO3 at 1 µg/mL, which exhibited a significantly lower survival rate of 54% ($p = 0.0235$) (Fig. 8).

To gain a deeper insight into the toxicity observed in larvae, oxidative stress assays were conducted. The results demonstrated that the levels of ROS and FRAP remained comparable to those observed in the water control across the tested treatments (Fig. 9A and B). AOPP levels were found to be significantly elevated in larvae exposed to WSF-AgNPs at 100 µg/mL ($p = 0.0051$), whereas a reduction was observed in larvae exposed to < 10 kDa-AgNPs at the same concentration ($p = 0.0054$) in comparison to the water control (Fig. 9C). The sulfhydryl content was found to be significantly elevated in larvae exposed to WSF-AgNPs at 100 µg/mL ($p = 0.0037$) in comparison to the water control (Fig. 9D). The activity of SOD was found to be significantly reduced in larvae exposed to WSF-AgNPs at 10 µg/mL ($p = 0.0002$), as well as in larvae exposed to < 10 kDa-

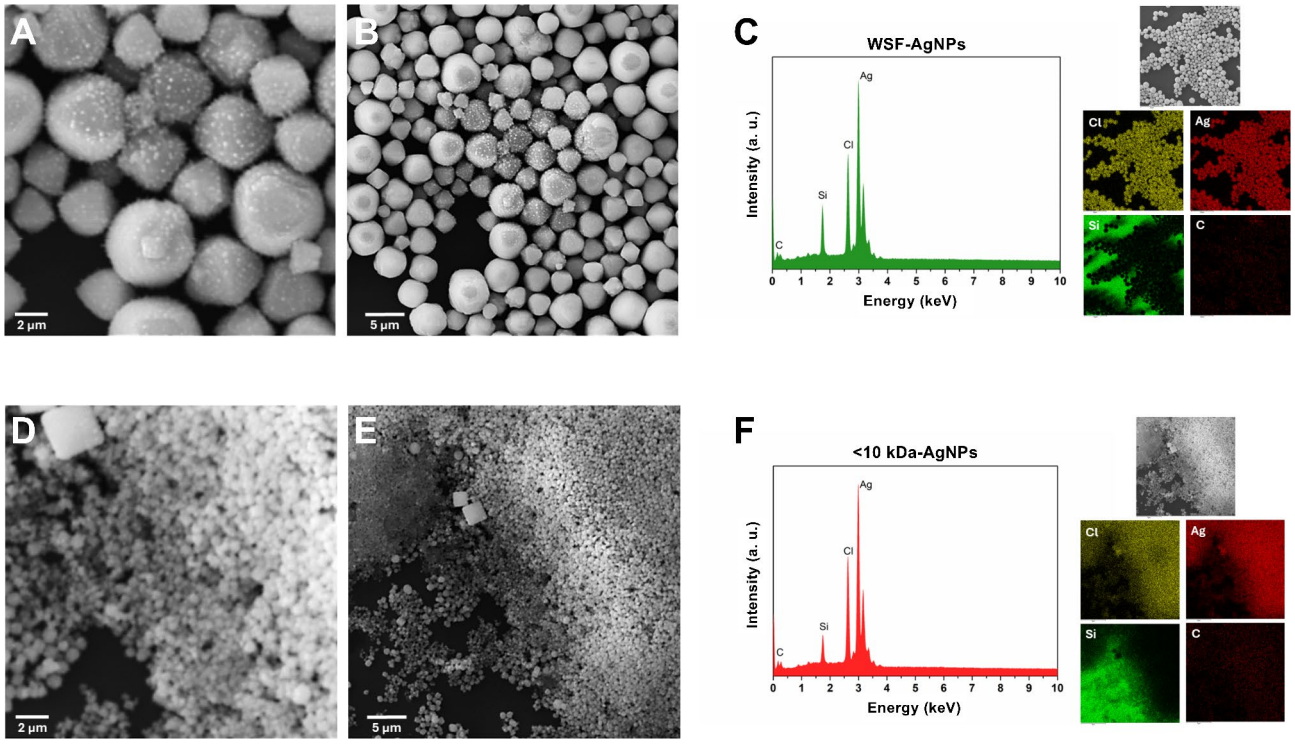

Fig. 6. **Scanning electron microscopy (SEM) and energy-dispersive X-ray spectroscopy (EDX) analysis.** The SEM images of WSF-AgNPs display their predominantly spherical morphology and a polydisperse distribution, with nanoparticle sizes ranging from 500 to 1000 nm, consistent with DLS analysis (**A** and **B**). EDX spectroscopy of these nanoparticles confirms the presence of carbon, chloride, and silver in their composition (**C**). Imaging of < 10 kDa-AgNPs corroborates the DLS findings, showing smaller particle sizes compared to WSF-AgNPs, with less variability, predominantly between 50 and 200 nm, though a few larger particles are observed (**D** and **E**). EDX analysis similarly identified carbon, chloride, and silver within these nanoparticles (F). It should be noted that silica was used as a base for SEM imaging and EDX, accounting for its presence in the spectra. Figures A and D show a magnification of 25,000x, while Figures B and E are magnified 10,000x.

Multidrug-resistant microorganisms	Inhibition Zone (mm ± SD)						
	WSF	WSF-AgNPs (µg/mL)			< 10 kDa-AgNPs (µg/mL)		
		10	100	1000	10	100	1000
A. baumannii	8.87 ± 0.304^{a}	$0^{aA\#}$	$8.777 \pm 0.240^{aB\#}$	$14.193 \pm 0.693^{bC\#}$	$0^{aA\#}$	$10.133 \pm 0.506^{bB*}$	$12.903 \pm 1.098^{bC*}$
E. coli	0^{a}	$0^{aA\#}$	$0^{aA\#}$	$10.173 \pm 0.456^{bB\#}$	$0^{aA\#}$	$6.98 \pm 0.046^{bB*}$	$10.173 \pm 0.482^{bC\#}$
K. pneumoniae	0^{a}	$0^{aA\#}$	$8.373 \pm 0.423^{bB\#}$	$9.783 \pm 0.446^{bC\#}$	$0^{aA\#}$	$7.213 \pm 0.405^{bB*}$	$9.993 \pm 0.444^{bC\#}$
***P. aeruginosa*IMP**	0^{a}	$0^{aA\#}$	$0^{aA\#}$	$9.807 \pm 0.514^{bB\#}$	$0^{aA\#}$	$0^{aA\#}$	$8.510 \pm 0.572^{bB*}$
***P. aeruginosa*SPM**	0^{a}	$0^{aA\#}$	$0^{aA\#}$	$9.717 \pm 0.321^{bB\#}$	$0^{aA\#}$	$0^{aA\#}$	$9.643 \pm 0.179^{bB\#}$
***P. aeruginosa*VIM**	0^{a}	$0^{aA\#}$	$0^{aA\#}$	$9.610 \pm 0.937^{bB\#}$	$0^{aA\#}$	$0^{aA\#}$	$8.627 \pm 0.263^{bB\#}$
S. aureus	0^{a}	$0^{aA\#}$	$0^{aA\#}$	$9.037 \pm 0.127^{bB\#}$	$0^{aA\#}$	$8.237 \pm 0.585^{bB*}$	$11.617 \pm 0.391^{bC*}$

Table 1. **Assessment of bacterial growth Inhibition via the diffusion disk technique.** The WSF-AgNPs inhibited the growth of *A. baumannii* and *K. pneumoniae* at a concentration of 100 µg/ml. At a concentration of 1000 µg/ml, they inhibited the growth of all tested bacteria. The < 10 kDa-AgNPs inhibited the growth of *A. baumannii*, *E. coli*, *K. pneumoniae*, and *S. aureus* at 100 µg/ml.and inhibited the growth of all tested bacteria at 1000 µg/ml. Inhibition zones values of 0 indicate that they were absent. Lowercase letters indicate significant differences between AgNPs and WSF. The capital letters indicate significant differences among different concentrations of the same AgNPs. Symbols indicate significant differences among the same concentration of different AgNPs. Statistics were calculated by two-way ANOVA. All differences shown have a P value < 0.0001.

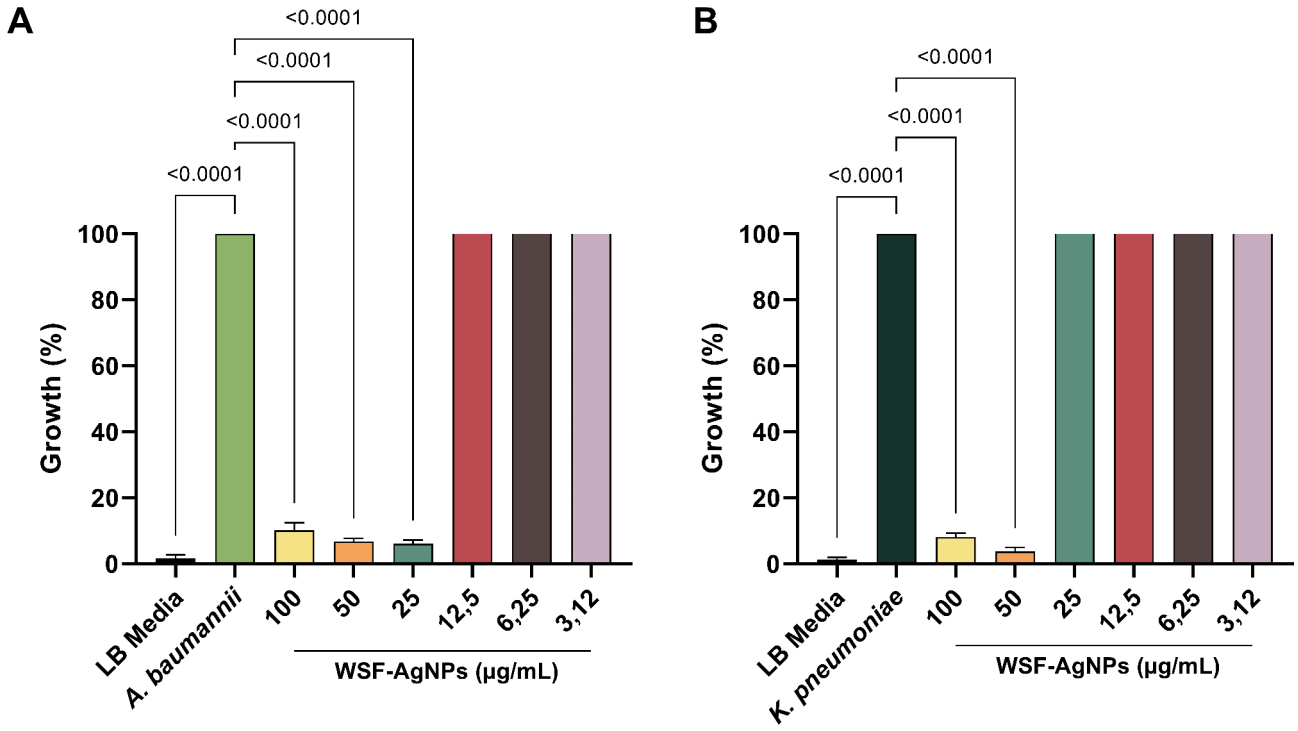

Fig. 7. **Minimum inhibitory concentration assessment for WSF-AgNPs.** The WSF-AgNPs demonstrated inhibitory effects on the growth of A. baumannii at concentrations of 100, 50, and 25 µg/mL (**A**), with the MIC determined to be 25 µg/mL. Inhibition was observed for K. pneumoniae at concentrations of 100 and 50 µg/mL, with the MIC set at 50 µg/mL (**B**). Each treatment was tested in six replicates, and statistical analysis was performed using one-way ANOVA followed by Dunnett's multiple comparisons test. Brackets indicate statistically significant differences, along with the corresponding p-values. The data are presented in the graph as mean ± standard deviation.

Treatments	Expected (No. of Embryos)	Observed (No. of Adults)	*p*-value (vs. Water)
Water	102	54	–
WSF	125	74	0.6166
$AgNO_3$100 µg/mL	115	0	**< 0.0001**
$AgNO_3$10 µg/mL	105	33	**0.0448**
$AgNO_3$1 µg/mL	116	56	0.6935
WSF-AgNPs 100 µg/mL	114	28	**0.0146**
WSF-AgNPs 10 µg/mL	117	89	0.0979
WSF-AgNPs 1 µg/mL	106	52	0.7495
< 10 kDa-AgNPs 100 µg/mL	109	33	**0.0031**
< 10 kDa-AgNPs 10 µg/mL	124	59	0.6438
< 10 kDa-AgNPs 1 µg/mL	112	61	0.9025

Table 2. **Analysis of different treatments on the development of*Drosophila melanogaster***. The table displays the expected number of adult individuals, based on the initial number of embryos introduced to the medium prepared with each treatment, and the observed number of adults that emerged from each treatment vial seven days after the first eclosion. The column labeled "p-value (vs. Water)" denotes the statistical significance of the discrepancy in the number of emerging adults between each treatment and the water group (negative control), as determined through a two-sided chi-square test. Bold p-values represent statistically significant differences.

AgNPs at 1 µg/mL ($p = 0.0032$) and 100 µg/mL ($p < 0.0001$), in comparison to the control group (Fig. 9E). Furthermore, no alterations in CAT activity were observed in any of the treated groups in comparison to the control group (Fig. 9F). The GSH content was markedly elevated in larvae exposed to WSF-AgNPs at 100 µg/mL ($p = 0.0002$) in comparison to the water control (Fig. 9G).

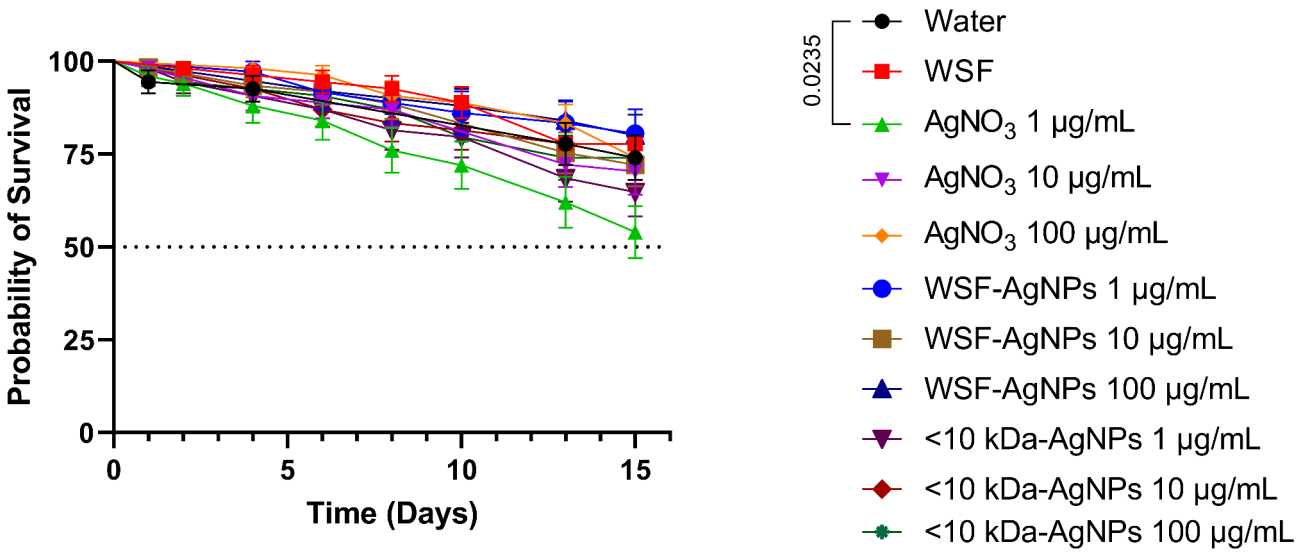

Fig. 8. **Toxicity assessment on adult*Drosophila melanogaster*flies.** In comparison to the negative control (distilled water), only the $AgNO_3$ treatment at 1 µg/mL exhibited significant toxicity, with a survival rate of 54%. This toxicity assessment was conducted using 20 flies of the w^{1118} strain of *Drosophila melanogaster* (10 males and 10 females) aged 0–2 days post-emergence. The survival analysis was performed using the Log-rank (Mantel-Cox) test, and the bracket indicates statistically significant differences between groups, with the associated p-value. The error bars in the graph represent the standard error of the survival estimates.

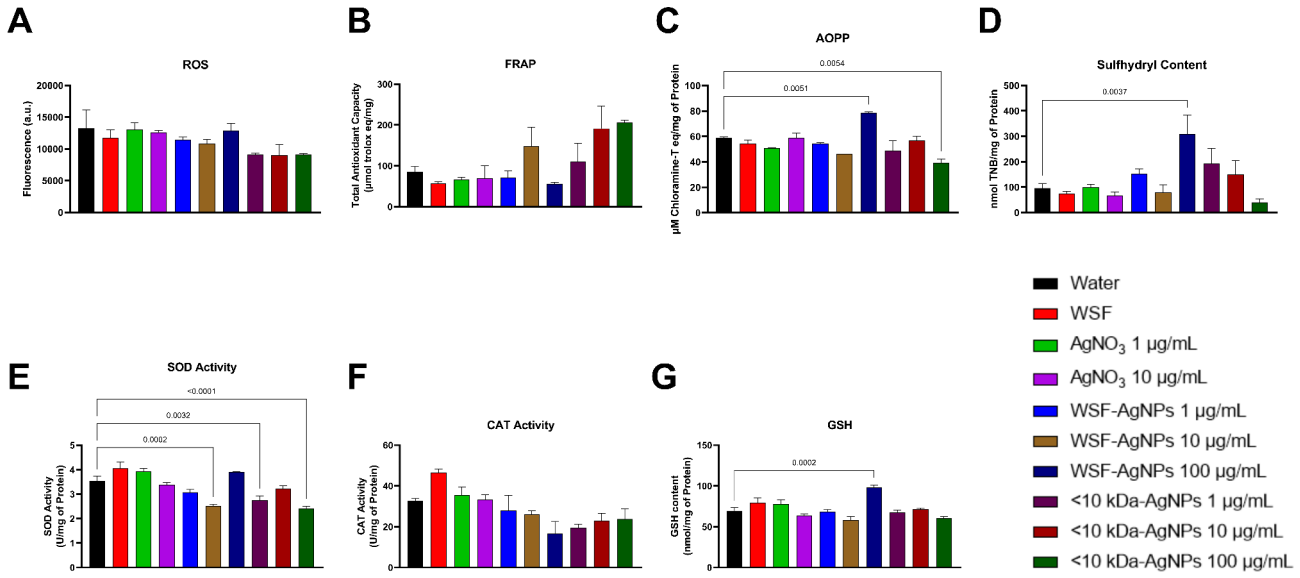

Fig. 9. Oxidative stress analysis in *Drosophila melanogaster* larvae exposed to AgNPs. The results demonstrated no significant differences in ROS and FRAP levels across the treatment groups in comparison to the water control group (**A** and **B**). AOPP levels were found to be significantly elevated in larvae treated with WSF-AgNPs at 100 µg/mL ($p = 0.0051$) and decreased in those treated with < 10 kDa-AgNPs at 100 µg/mL ($p = 0.0054$) in comparison to the water control (**C**). The sulfhydryl content was found to be significantly elevated in larvae treated with WSF-AgNPs at 100 µg/mL ($p = 0.0037$) in comparison to the water control (**D**). The activity of SOD was significantly diminished in larvae treated with WSF-AgNPs at 10 µg/mL ($p = 0.0002$) and in those treated with < 10 kDa-AgNPs at 1 µg/mL ($p = 0.0032$) and 100 µg/mL ($p < 0.0001$) in comparison to the water control (**E**). No significant alterations in CAT activity were observed across any treatments (**F**). GSH content was significantly increased in larvae treated with WSF-AgNPs at 100 µg/mL ($p = 0.0002$) compared to the water control (**G**). The data are presented as mean ± standard error of the mean ($n = 3$ biological replicates, 40 larvae each), and were analyzed using one-way ANOVA with Dunnett's post-test. The presence of brackets indicates statistically significant differences alongside their p-values.

Discussion

The therapeutic effects of kefir have been explored in medicine because of its ability to treat many medical conditions, from neurological to gut diseases[41–43]. Although the existing literature extensively covers the therapeutic benefits of kefir, there is a gap in research regarding the utilization of nanotechnology to enhance kefir's effects through the production of nanoparticles. In previous studies conducted by our research group, both the WSF and the < 10 kDa fraction of kefir demonstrated antioxidant activity in an in vitro FRAP assay, with the latter exhibiting a higher antioxidant potential[19]. Based on these results, we identified its potential as a reducing agent for silver in a green synthesis of nanoparticles. Therefore, our research aimed to evaluate the use of kefir's WSF and < 10 kDa fraction in the green synthesis of silver nanoparticles, assessing their potential to enhance kefir's therapeutic benefits, particularly its antimicrobial activities.

The AgNPs synthesized from both kefir fractions exhibited a spherical-like morphology, with the particles obtained from the < 10 kDa fraction being notably smaller in size. Both AgNPs demonstrated a −30 mV mean zeta potential. WSF-AgNPs demonstrated antimicrobial activity against *A. baumannii* and *K. pneumoniae* at concentrations of 25 and 50 µg/mL, respectively. Furthermore, toxicity was observed only in the post-embryonic development of *Drosophila melanogaster*, not in adults at the tested concentrations. Our oxidative stress analysis revealed a mild imbalance, suggesting that the observed toxicity may result from mechanisms other than oxidative damage.

The nanoparticles were comprehensively characterized using UV–Vis spectroscopy, DLS, and FT-IR spectroscopy. Silver nanoparticles typically exhibit a distinct absorbance peak in the 400–500 nm range in UV-Vis spectra[44–47]. The results of our UV-Vis spectroscopy analysis demonstrated that the distinctive peak was exclusively present in our WSF-AgNPs, but not in the < 10 kDa-AgNPs. It is hypothesized that the < 10 kDa-AgNPs, due to their smaller size, may exhibit a broader absorbance, resulting in the absence of a distinct peak. Additionally, it is possible that these nanoparticles are composed of silver oxide (Ag_2O or AgO), which also exhibit a broader absorbance range, rather than metallic silver. Further investigation is required to explain the lack of distinct absorbance peaks in the < 10 kDa-AgNPs.

The GC-MS results demonstrated the presence of a diverse array of compounds in the WSF, including fatty acids, phenols, and fermentation-specific compounds. These findings are consistent with those from previous studies by our research group[20], which can be correlated with specific bands observed in the FT-IR spectrum from this study. Among the identified compound families, fatty acids, such as n-hexadecanoic and octadecanoic acids, are likely responsible for the band observed between 1700 and 1750 cm^{-1}, which is attributed to the C = O vibration of carbonyl groups[48]. The presence of fatty amides may be associated with the band observed between 1500 and 1700 cm^{-1}, which aligns with the N-H and C = O vibrations characteristic of both amides and peptides[48]. Moreover, the presence of phenolic compounds is known to contribute to the peaks observed in the 1000–1300 cm^{-1} range, which are attributed to C-O and C-N vibrations[49].

Some of the compounds identified by GC-MS are known to be metabolites of fermentation, that is to say, they are not present in milk but are specific to kefir. Examples of these compounds include 2,4-di-tert-butylphenol (2,4-DTBP), 1-heptadecanamine and 9-octadecenamide (Z)-, which were found to be more abundant in our kefir sample[50–52]. Of these three, 2,4-DTBP has been the subject of the most research, with studies describing its antioxidant, antibacterial, anti-inflammatory and anti-fungal activities[53].

The biochemical complexity observed by FT-IR reflects the intricate profile of compounds present in WSF. It is noteworthy that the band observed between 1500 and 1700 cm^{-1} was the only one also present in the synthesized nanoparticles. This suggests that metabolites with these functional groups, along with bioactive peptides derived from WSF, were the primary contributors to nanoparticle formation, acting as reducing agents for silver during synthesis. These findings underscore the pivotal role of specific functional groups in the stabilization and reduction processes of AgNP synthesis.

Optimizing the parameters for DLS was crucial due to the limited insight provided by the literature and equipment manuals on key parameters and equipment settings[54]. For instance, the equipment manual recommends using backscatter measurements for concentrated samples, but it does not provide specific concentration guidelines. Furthermore, information on parameters such as transmittance and baseline are not well explored in the literature. These parameters are utilized to assess the reliability of the collected data, leaving room for further knowledge.

To address this gap, our study conducted rigorous testing across various sample concentrations to determine the most effective parameters for reliable analysis of our samples. This empirical approach yielded valuable insights into the influence of concentration and equipment settings on measurement outcomes. The findings provide important guidance for future research aiming to accurately characterize silver nanoparticles based on sample properties.

The hydrodynamic radius of our AgNPs (WSF-AgNPs: 1201 nm and < 10 kDa-AgNPs: 481.6 nm) is larger than that reported in previous syntheses[55,56]. However, improving the biological synthesis process of AgNPs—by testing different pH, precursor concentrations, temperature, and exposure to light—can affect their physical characteristics, such as size, shape, and PDI[57]. Future research will aim to optimize the synthesis process and analyze the outcomes resulting from varying these parameters.

The PDI of nanoparticles is a critical factor in drug delivery efficacy and safety[58]. Notably, the synthesized < 10 kDa-AgNPs fall within the acceptable PDI range (below 30%)[58], allowing for more precise studies of potential side effects and the optimization for drug delivery purposes. Furthermore, our AgNPs exhibited a zeta potential of around − 30 mV, indicating that they are stable and have minimal tendency to aggregate[59].

The size and shape of nanoparticles can influence their uptake by cells and their interaction within biological systems, and consequently their toxicity. The WSF-AgNPs exhibit a size range of 500 to 1000 nm, while the < 10 kDa-AgNPs display a size range of 100 to 200 nm, with some nanoparticles measuring approximately

400 nm. Given that, according to the literature, smaller nanoparticles tend to have higher absorption rates[60,61], it is anticipated that the < 10 kDa-AgNPs will exhibit a higher rate of absorption compared to the WSF-AgNPs. With regard to their shape, spherical nanoparticles can enter tissues more easily than other shapes. However, the data in the literature remains inconsistent, and further studies are needed to ascertain the effects of different nanoparticle shapes on their uptake[61].

In our toxicity assessment, during the post-embryonic stage, both WSF-AgNPs and < 10 kDa-AgNPs demonstrated significant toxicity at the highest concentration tested (100 µg/mL), as evidenced by the reduced number of emerging adults, which suggests that exposure to higher concentrations of AgNPs during early developmental stages can severely impair growth and survival. Conversely, the adult toxicity assessment showed no reduction in survival rates for any AgNP treatment, even at the same concentration of 100 µg/mL. The absence of toxicity in adults, despite the adverse effects observed during early stages, highlights potential differences in the susceptibility of *Drosophila melanogaster* to these treatments across life stages.

A closer examination of the toxicity observed in larvae revealed that those that ingested the AgNPs exhibited moderate oxidative stress, as indicated by the oxidative stress analysis. This analysis also revealed a reduction in SOD activity at concentrations of 10 and 100 µg/mL, as well as an increase in AOPP levels at 100 µg/mL for the WSF-AgNPs. In contrast, the 10 kDa-AgNPs exhibited less pronounced effects, with a diminished impact on SOD activity and even a decline in AOPP levels at 100 µg/mL. Furthermore, an increase in GSH content was observed in larvae exposed to WSF-AgNPs at 100 µg/mL, which may represent a compensatory response to counteract oxidative damage induced by the AgNPs. However, the absence of significant changes in ROS and FRAP levels, as well as the unaltered CAT activity, suggests that the toxicity of the AgNPs in larvae might not be solely attributed to oxidative stress but could involve other mechanisms or pathways.

It is hypothesized that the AgNPs could act as hormonal disruptors, interfering with critical processes such as the synthesis and regulation of hormones essential for metamorphosis. This hypothesis is supported by the observed mortality of larvae in intermediate developmental stages, prior to the transition to the pupal phase, and by the absence of severe impacts on adults, which have already completed these processes. Therefore, our findings suggest that the toxicity of the AgNPs may be related to indirect effects on development. However, further studies are needed to investigate these pathways and clarify this hypothesis.

These findings are consistent with those of previous research conducted by our group, in which silver nanoparticles produced using pollen extract and employing the same methodology did not demonstrate any toxicity to adult flies[30], and those produced by other groups using natural products as the source for their nanoparticle synthesis[28,29]. However, it should be noted that fruit flies serve only as a preliminary trial model organism, and further research is necessary on chordate animals to more accurately assess the toxicity of the nanoparticles produced from the water-soluble fraction of kefir.

A number of studies have demonstrated that AgNPs synthesized via green methods, such as the use of plant extracts and pollen, display antimicrobial activity against bacterial and fungal pathogens[30,62–65], which supports our findings. Although both the WSF-AgNPs and < 10 kDa-AgNPs produced inhibition zones against all test bacteria at 1000 µg/mL, it is worth mentioning that this concentration is very high and would be expected to produce inhibition zones. High concentrations of antimicrobials can be toxic to users, and lack of specificity can lead to microbial resistance[66–68]. Thus, the importance of determining the minimum inhibitory concentration for these nanoparticles.

The MIC assay revealed that WSF-AgNPs effectively inhibited the growth of *A. baumannii* at a concentration of 25 µg/mL and *K. pneumoniae*at 50 µg/mL. These results highlight potential applications for these AgNPs, such as in sterilizing solutions or as coatings for medical materials, approaches that have been explored in previous studies involving AgNPs[69–71].

In contrast, the < 10 kDa-AgNPs exhibited instability during the MIC assay, thereby failing to produce consistent antibacterial effects. Although these nanoparticles demonstrated inhibitory activity in the in vitro disk diffusion assay against *A. baumannii*, *K. pneumoniae*, *E. coli*, and *S. aureus* at 100 µg/mL, MIC testing yielded inconsistent results across multiple repetitions and nanoparticle batches. These findings underscore the need for further investigation into the stability and reproducibility of < 10 kDa-AgNPs, particularly in antimicrobial assays, to better understand their potential applications.

In future research, we plan to investigate the feasibility of incorporating our WSF-AgNPs into disinfectant solutions with the aim of achieving effective decontamination[71]. Moreover, we will undertake an examination of the impact of kefir derived-AgNPs on wound healing processes, with a particular emphasis on their capacity to facilitate superior skin regeneration and serve as a healing agent and antiseptic. Finally, we aim to conduct drug development tests to explore novel avenues for antibiotic production, capitalizing on the distinctive properties possessed by these AgNPs.

It is important to acknowledge the limitations of this research. Firstly, the production of AgNPs from kefir, a natural product, may be subject to variation due to differences in the bioactive components of kefir sourced from different batches. Moreover, although no toxicity was observed in adult *Drosophila melanogaster*, further studies are required to assess the effects of AgNPs on specific organ of this model organism. Additionally, in vivo studies in higher organisms and clinical trials are essential to confirm the safety and efficacy of these AgNPs in humans. Our group plans to conduct a more thorough toxicity evaluation in *Drosophila melanogaster* in future research.

Conclusion

The present study corroborates the hypothesis that the antioxidant-rich, water-soluble fraction of kefir serves as an effective reducing agent for the green synthesis of silver nanoparticles (AgNPs). Moreover, AgNPs derived from both the WSF and the < 10 kDa fractions were demonstrated to enhance the antimicrobial activity of kefir's water-soluble fraction. The successful synthesis of AgNPs was verified by UV-visible and FT-IR spectroscopy, with DLS and SEM imaging providing key insights into size distribution, stability, and morphology. The in vitro

assays demonstrated the efficacy of WSF- and < 10 kDa-AgNPs in inhibiting the growth of multidrug-resistant bacteria. In the MIC assay, only WSF-AgNPs produced consistent results, exhibiting bactericidal activity against *A. baumannii* at 25 µg/mL *and K. pneumoniae* at 50 µg/mL. While the in vivo experiments showed that exposure to AgNPs impaired larval development in *Drosophila melanogaster*, no toxicity was observed in adult flies after prolonged exposure. These findings underscore the potential of green-synthesized AgNPs derived from different kefir's fractions in clinical applications, including topical antimicrobial agents, disinfectants, and coatings for medical devices. Future research will include further toxicity evaluations, with a focus on potential morphological changes in specific model organisms organs. Additionally, efforts will be made to enhance specificity through compound conjugation and to explore broader applications in drug development.

Data availability

The datasets produced or analyzed during the current study are available from the corresponding author upon request.

Received: 30 July 2024; Accepted: 24 March 2025
Published online: 27 March 2025

References

1. Simon, S. et al. Biomedical applications of plant Extract-Synthesized silver nanoparticles. *Biomedicines* ;**10**. (2022).
2. Rabiee, N., Ahmadi, S., Akhavan, O. & Luque, R. Silver and gold nanoparticles for antimicrobial purposes against Multi-Drug resistance bacteria. *Mater. (Basel)* ;**15**. (2022).
3. More, P. R. et al. Silver nanoparticles: bactericidal and mechanistic approach against drug resistant pathogens. *Microorganisms* **11**, 369 (2022).
4. Aljeldah, M. M., Aboul-Soud, M. A. M., Yassin, M. T. & Mostafa, A. A. F. Synergistic antibacterial potential of Greenly synthesized silver nanoparticles with fosfomycin against some nosocomial bacterial pathogens. *Infect. Drug Resist.* **16**, 125–142 (2023).
5. Macovei, I. et al. Phyto-functionalized silver nanoparticles derived from conifer bark extracts and evaluation of their antimicrobial and cytogenotoxic effects. *Molecules* ;**27**. (2022).
6. Ghetas HA, Abdel-Razek N, Shakweer MS, Abotaleb MM, Ahamad Paray B, Ali S, et al. Antimicrobial activity of chemically and biologically synthesized silver nanoparticles against some fish pathogens. Saudi J Biol Sci [Internet]. 2022;29:1298–305. Available from: https://doi.org/10.1016/j.sjbs.2021.11.015
7. Al-Otibi, F. O., Yassin, M. T., Al-Askar, A. A. & Maniah, K. Green biofabrication of silver nanoparticles of potential synergistic activity with antibacterial and antifungal agents against some nosocomial pathogens. *Microorganisms* ;11. (2023).
8. Naganthran, A. et al. Synthesis, characterization and biomedical application of silver nanoparticles. *Mater. (Basel).* **15**, 1–43 (2022).
9. Almatroudi, A. Silver nanoparticles: synthesis, characterisation and biomedical applications. *Open. Life Sci.* **15**, 819–839 (2020).
10. Sharma, N. K. et al. Green route synthesis and characterization techniques of silver nanoparticles and their biological adeptness. *ACS Omega*. **7**, 27004–27020 (2022).
11. Kummara S, Patil MB, Uriah T. Synthesis, characterization, biocompatible and anticancer activity of green and chemically synthesized silver nanoparticles – A comparative study. Biomed Pharmacother [Internet]. 2016;84:10–21. Available from: http://dx.doi.org/10.1016/j.biopha.2016.09.003
12. Sampath, G. et al. Biologically synthesized silver nanoparticles and their diverse applications. *Nanomaterials* ;**12**. (2022).
13. Shivani Tiwari, Jyotsna Gade, A. C. Research Article biosynthesis of silver nanoparticles using Bacillus Sp. for microbial disease control: an in-vitro and in-silico approach. *Sch. Acad. J. Pharm.* **4**, 389–397 (2015).
14. Feroze, N. et al. Fungal mediated synthesis of silver nanoparticles and evaluation of antibacterial activity. *Microsc Res. Tech.* **83**, 72–80 (2020).
15. Culpepper, T. The effects of Kefir and Kefir components on immune and metabolic physiology in Pre-Clinical studies: A narrative review. *Cureus* **14**, 1–9 (2022).
16. González-Orozco, B. D., García-Cano, I., Jiménez-Flores, R. & Alvárez, V. B. Invited review: milk Kefir microbiota—Direct and indirect antimicrobial effects. *J. Dairy. Sci.* **105**, 3703–3715 (2022).
17. Azizi, N. F. et al. Kefir and its biological activities. *Foods* **10**, 1–26 (2021).
18. Taheur F Ben, Mansour C, Chaieb K. Inhibitory effect of kefir on Aspergillus growth and mycotoxin production. Euro-Mediterranean J Environ Integr [Internet]. 2020;5:1–8. Available from: https://doi.org/10.1007/s41207-020-0141-x
19. Malta SM, Batista LL, Silva HCG, Franco RR, Silva MH, Rodrigues TS, et al. Identification of bioactive peptides from a Brazilian kefir sample, and their anti-Alzheimer potential in Drosophila melanogaster. Sci Rep [Internet]. 2022;12:1–12. Available from: https://doi.org/10.1038/s41598-022-15297-1
20. 20. Batista LL, Malta SM, Guerra Silva HC, Borges LDF, Rocha LO, da Silva JR, et al. Kefir metabolites in a fly model for Alzheimer's disease. Sci Rep [Internet]. 2021;11:1–12. Available from: https://doi.org/10.1038/s41598-021-90749-8
21. Vijayaram S, et al. Applications of Green Synthesized Metal Nanoparticles — a Review. Biol Trace Elem Res [Internet]. 2023; Available from: https://doi.org/10.1007/s12011-023-03645-9
22. Nicolae-Maranciuc, A., Chicea, D. & Chicea, L. M. Ag nanoparticles for biomedical Applications-Synthesis and Characterization-A review. *Int. J. Mol. Sci.* ;**23**. (2022).
23. Mandal, A. K. et al. Current research on zinc oxide nanoparticles: synthesis, characterization, and biomedical applications. *Nanomaterials* ;12. (2022).
24. Begum, S. J. P. et al. Recent advances in green synthesis, characterization, and applications of bioactive metallic nanoparticles. *Pharmaceuticals* **15**, 1–20 (2022).
25. Noga, M., Milan, J., Frydrych, A., Jurowski, K. & Toxicological Aspects Safety assessment, and green toxicology of silver nanoparticles (AgNPs)—Critical review: state of the Art. *Int. J. Mol. Sci.* ;**24**. (2023).
26. Ferdous, Z. & Nemmar, A. Health impact of silver nanoparticles: A review of the biodistribution and toxicity following various routes of exposure. *Int. J. Mol. Sci.* (2020).
27. Lopez-Ortiz, C. et al. Drosophila melanogaster as a translational model system to explore the impact of phytochemicals on human health. *Int. J. Mol. Sci.* ;**24**. (2023).
28. Desai, A. S. et al. An in vitro and in vivo study of the efficacy and toxicity of Plant-Extract-Derived silver nanoparticles. *J. Funct. Biomater.* ;**13**. (2022).
29. Singh, M. P. et al. Synthesis of green engineered silver nanoparticles through urtica Dioica: an Inhibition of microbes and alleviation of cellular and organismal toxicity in drosophila melanogaster. *Antibiotics* ;**11**. (2022).
30. Santos ACC, et al. Green synthesis of silver nanoparticle using pollen extract from Tetragonisca angustula a stingless bee. Discov Nano [Internet]. 2024;19. Available from: https://doi.org/10.1186/s11671-024-04038-0

31. Logaranjan K, Raiza AJ, Gopinath SCB, Chen Y, Pandian K. Shape- and Size-Controlled Synthesis of Silver Nanoparticles Using Aloe vera Plant Extract and Their Antimicrobial Activity. Nanoscale Res Lett [Internet]. 2016;11. Available from: http://dx.doi.org/10.1186/s11671-016-1725-x
32. Hudzicki, J. Kirby-Bauer Disk Diffusion Susceptibility Test Protocol Author Information. Am Soc Microbiol [Internet]. ;1–13. (2012). Available from: https://www.asm.org/Protocols/Kirby-Bauer-Disk-Diffusion-Susceptibility-Test-Pro
33. Kourmouli, A. et al. Can disc diffusion susceptibility tests assess the antimicrobial activity of engineered nanoparticles? *J. Nanoparticle Res.* **20**, 2–7 (2018).
34. Bio-Rad Antibodies. General Method for Measuring Cytotoxicity or Proliferation Using alamarBlue [Internet]. [cited 2024 Nov 12]. p. 1. Available from: https://www.bio-rad-antibodies.com/measuring-cytotoxicity-proliferation-spectrophotometry-fluorescence-alamarblue.html
35. Bradford, M. M. A rapid and sensitive method for the quantitation of microgram quantities of protein utilizing the principle of protein-dye binding. *Anal. Biochem.* **72**, 248–254 (1976).
36. Myers AL, Harris CM, Choe KM, Brennan CA. Inflammatory production of reactive oxygen species by Drosophila hemocytes activates cellular immune defenses. Biochem Biophys Res Commun [Internet]. 2018;505:726–32. Available from: https://doi.org/10.1016/j.bbrc.2018.09.126
37. Witko-Sarsat, V. et al. Advanced oxidation protein products as a novel marker of oxidative stress in uremia. *Kidney Int.* **49**, 1304–1313 (1996).
38. Ellman, G. L. Tissue sulfhydryl groups. *Arch. Biochem. Biophys.* **82**, 70–77 (1959).
39. Marklund, S. & Marklund, G. Involvement of the superoxide anion radical in the autoxidation of pyrogallol and a convenient assay for superoxide dismutase. *Eur. J. Biochem.* **47**, 469–474 (1974).
40. Aebi, H. Catalase in vitro. Methods Enzymol. (1984).
41. Ton, A. M. M. et al. Oxidative Stress and Dementia in Alzheimer's Patients: Effects of Synbiotic Supplementation. Oxid Med Cell Longev. ;2020. (2020).
42. Farag, M. A., Jomaa, S. A., El-Wahed, A. A. & El-Seedi, H. R. The Many Faces of Kefir Fermented Dairy Products: Quality Characteristics, Flavour Chemistry, Nutritional Value, Health Benefits, and Safety. Nutrients [Internet]. ;12:346. (2020). Available from: www.mdpi.com/journal.nutrients
43. Vieira, C. P. et al. Bioactive Compounds from Kefir and Their Potential Benefits on Health: A Systematic Review and Meta-Analysis. Oxid Med Cell Longev. ;2021. (2021).
44. Durval, I. J. B. et al. Green synthesis of silver nanoparticles using a biosurfactant from Bacillus cereus UCP 1615 as stabilizing agent and its application as an antifungal agent. *Fermentation* **7**, 1–9 (2021).
45. Kaur, G., Sati, S. C., Mir, M. A. & Tripathi, P. K. Synthesis of silver nanoparticles using ficus Palmata leaves extract: characterization and evaluation for its antimicrobial and antioxidant activities. *Asian J. Pharm. Pharmacol.* **4**, 192–198 (2018).
46. Rudakiya, D. M. & Pawar, K. Bactericidal potential of silver nanoparticles synthesized using cell-free extract of Comamonas acidovorans: in vitro and in Silico approaches. *3 Biotech.* **7**, 1–12 (2017).
47. Allam NG, Ismail GA, El-Gemizy WM, Salem MA. Biosynthesis of silver nanoparticles by cell-free extracts from some bacteria species for dye removal from wastewater. Biotechnol Lett [Internet]. 2019;41:379–89. Available from: https://doi.org/10.1007/s10529-019-02652-y
48. Gul, A. et al. Protein Kinase Inhibition, Antibacterial Activity, and Characterization of Phytoextract-Mediated Silver Nanoparticles Using Aqueous Extracts of Ifloga spicata. J Nanomater. ;2022. (2022).
49. Netai, M. M., Jameson, K. & Mark, F. Z. Surface composition and surface properties of water hyacinth (Eichhornia crassipes) root biomass: effect of mineral acid and organic solvent treatment. *Afr. J. Biotechnol.* **15**, 897–909 (2016).
50. Seenivasan A, Manikkam R, Kaari M, Sahu AK, Said M, Dastager SG. 2,4-Di-tert-butylphenol (2,4-DTBP) purified from Streptomyces sp. KCA1 from Phyllanthus niruri: Isolation, characterization, antibacterial and anticancer properties. J King Saud Univ - Sci [Internet]. 2022;34:102088. Available from: https://doi.org/10.1016/j.jksus.2022.102088
51. Ren Q, Sun L, Wu H, Wang Y, Wang Z, Zheng F, et al. The changes of microbial community and flavor compound in the fermentation process of Chinese rice wine using Fagopyrum tataricum grain as feedstock. Sci Rep [Internet]. 2019;9:1–12. Available from: http://dx.doi.org/10.1038/s41598-019-40337-8
52. Jiang, S. et al. The products from fermentation of wheat Bran fiber by auricularia polytricha strain and the effects of the products on rheological properties of dough sheet. *Food Sci. Nutr.* **8**, 1345–1354 (2020).
53. Zhao, F., Wang, P., Lucardi, R. D., Su, Z. & Li, S. Natural sources and bioactivities of 2,4-di-tert-butylphenol and its analogs. *Toxins (Basel).* **12**, 1–26 (2020).
54. Bellmann, C., Caspari, A., Moitzi, C. & Babick, F. *Dynamic and Electrophoretic Light Scattering* 3rd edn. (Anton Paar GmbH, 2020).
55. Gemishev, O., Panayotova, M., Gicheva, G. & Mintcheva, N. Green synthesis of stable spherical monodisperse silver nanoparticles using a Cell-Free extract of trichoderma Reesei. *Mater. (Basel)* ;15. (2022).
56. Singh, Y., Kaushal, S. & Sodhi, R. S. Biogenic synthesis of silver nanoparticles using cyanobacterium: leptolyngbya Sp. WUC 59 cell-free extract and their effects on bacterial growth and seed germination. *Nanoscale Adv.* **2**, 3972–3982 (2020).
57. Bao, Z., Cao, J., Kang, G. & Lan, C. Q. Effects of reaction conditions on light-dependent silver nanoparticle biosynthesis mediated by cell extract of green Alga Neochloris oleoabundans. *Environ. Sci. Pollut Res.* **26**, 2873–2881 (2019).
58. Danaei, M. et al. Impact of particle size and polydispersity index on the clinical applications of lipidic nanocarrier systems. *Pharmaceutics* **10**, 1–17 (2018).
59. Manosalva N, Tortella G, Cristina Diez M, Schalchli H, Seabra AB, Durán N, et al. Green synthesis of silver nanoparticles: effect of synthesis reaction parameters on antimicrobial activity. World J Microbiol Biotechnol [Internet]. 2019;35. Available from: https://doi.org/10.1007/s11274-019-2664-3
60. Banerjee, A., Qi, J., Gogoi, R., Wong, J. & Mitragotri, S. Role of nanoparticle size, shape and surface chemistry in oral drug delivery. *J. Control Release.* **238**, 176–185 (2016).
61. Wang, Y. et al. The influence of nanoparticle properties on oral bioavailability of drugs. *Int. J. Nanomed.* **15**, 6295–6310 (2020).
62. Loo, Y. Y. et al. In vitro antimicrobial activity of green synthesized silver nanoparticles against selected Gram-negative foodborne pathogens. *Front. Microbiol.* **9**, 1–7 (2018).
63. Bahrulolum H, Nooraei S, Javanshir N, Tarrahimofrad H, Mirbagheri VS, Easton AJ, et al. Green synthesis of metal nanoparticles using microorganisms and their application in the agrifood sector. J Nanobiotechnology [Internet]. 2021;19:1–26. Available from: https://doi.org/10.1186/s12951-021-00834-3
64. Guilger-Casagrande M, Germano-Costa T, Bilesky-José N, Pasquoto-Stigliani T, Carvalho L, Fraceto LF, et al. Influence of the capping of biogenic silver nanoparticles on their toxicity and mechanism of action towards Sclerotinia sclerotiorum. J Nanobiotechnology [Internet]. 2021;19:1–18. Available from: https://doi.org/10.1186/s12951-021-00797-5
65. Mondal, A. H. et al. Anti-bacterial and anti-candidal activity of silver nanoparticles biosynthesized using citrobacter spp. Ms5 culture supernatant. *Biomolecules* **10**, 1–15 (2020).
66. Azevedo, M. M., Pinheiro, C., Yaphe, J. & Baltazar, F. Assessing the impact of a school intervention to promote students' knowledge and practices on correct antibiotic use. *Int. J. Environ. Res. Public. Health.* **10**, 2920–2931 (2013).
67. Zhong, W. et al. Designer broad-spectrum polyimidazolium antibiotics. *Proc. Natl. Acad. Sci. U S A.* **117**, 31376–31385 (2020).
68. Yan, J. et al. Chemical synthesis of innovative silver nanohybrids with synergistically improved antimicrobial properties. *Int. J. Nanomed.* **18**, 2295–2305 (2023).

69. Tahir I, Amina SJ, Ahmed NM, Janjua HA. Antimicrobial coating of biologically synthesized silver nanoparticles on surgical fabric and surgical blade to prevent nosocomial infections. Heliyon [Internet]. 2024;10:e35968. Available from: https://doi.org/10.1016/j.heliyon.2024.e35968
70. Elshahawy AM, Mahmoud GAE, Mokhtar DM, Ibrahim A. The optimal concentration of silver nanoparticles in sterilizing fish skin grafts. Sci Rep [Internet]. 2022;12:1–8. Available from: https://doi.org/10.1038/s41598-022-23853-y
71. Bruna, T., Maldonado-Bravo, F., Jara, P. & Caro, N. Silver nanoparticles and their antibacterial applications. *Int. J. Mol. Sci.* ;**22**. (2021).

Acknowledgements

We deeply appreciate all the assistance provided by Dr. Luiz Ricardo Goulart Filho, who tragically became one of the millions of victims of COVID-19.

Author contributions

LMMB: conceptualization; data curation; methodology; formal analysis; writing—original draft. SMM: data curation. ACCS: data curation. RADS: data curation. TSR: data curation. MNTDS: data curation. VPB: data curation. ALSB: data curation. ABJ: data curation. ABSN: data curation. MMM: data curation. FSE: data curation; methodology. APMS: conceptualization. CUV: conceptualization; methodology; funding acquisition; formal analysis; writing—review and editing. All authors reviewed the manuscript.

Funding

This project was funded by the Research Support Foundation of the State of Minas Gerais (FAPEMIG APQ-02766-17, APQ-00269-22 and National Council of Scientific and Technological Development (CNPq, grant number: 403193/2022-2) and FAPEMIG (grant number: CBB-APQ-03613-17) for INCT -TeraNano.

Declarations

Competing interests

The authors declare no competing interests.

Additional information

Supplementary Information The online version contains supplementary material available at https://doi.org/10.1038/s41598-025-95616-4.

Correspondence and requests for materials should be addressed to L.M.M.B. or C.U.-V.